Coronas and iridescence in mountain wave clouds

Joseph A. Shaw and Paul J. Neiman

We use Fraunhofer diffraction theory and meterological data to determine the nature of cloud-particle distributions and the mean particle sizes required for interpreting photographs of coronas and iridescence in mountain wave clouds. Traditional descriptions of coronas and iridescence usually explain these optical phenomena as diffraction by droplets of liquid water. Our analysis shows that the photographed displays have mean particle sizes from 7.6 to 24.3 μm, with over half the cases requiring diffraction by small (~20 μm) quasispherical ice particles rather than liquid water droplets. Previous documentation of coronas produced by ice particles are limited to observations in cirrus clouds that appear to be composed of small ice crystals, whereas our observations suggest that coronas and iridescence quite often can be created by tiny quasispherical ice particles that might be unique to mountain wave clouds. Furthermore, we see that the dominant colors in mountain wave-cloud coronas are red and blue, rather than the traditionally described red and green.

OCIS codes: 010.1290, 010.1310, 010.3920.

1. Introduction

When light from the Sun or the Moon passes through an optically thin cloud, scattering toward the forward direction can produce spectacular displays of color. Coronas and iridescence are two closely related colorful displays that can result from scattering in clouds.[1–7] A corona exhibits concentric colored rings around the light source, which range from blue or green on the inside to red on the outside. Iridescence is a more random, swirling patchwork of colors. The size, shape, and color purity of either display depend on the cloud particle size and distribution and on the optical thickness of the cloud. Generally the colors are of a pastel nature, with low purity, because of the high content of white light combined with the diffracted colors. These optical phenomena usually exist over an angular range of only several degrees around the light source, so they can be explained and analyzed by use of Fraunhofer diffraction theory. Circular (or quasi-circular) coronas with concentric colored rings centered on the light source are particularly amenable to this analysis. Coronas exhibit the traditional Fraunhofer diffraction inverse relationship between cloud particle size and corona-ring diameter. There is no similarly simple relationship that can be used to predict or analyze the random swirling patterns of iridescent clouds.

Mie scattering analysis by Lock and Yang[3] suggests that multiple-ring coronas can be visible when the cloud particle-size distribution is narrow and uniform throughout the cloud within several degrees of the light source, with a mean particle size of less than ~25 μm. A more random, swirling pattern of iridescence results when the mean particle size varies within the cloud region near the source or when the mean particle size is particularly small. Lock and Yang[3] used their scattering model for spherical water droplets to analyze corona photographs and found examples of visible multiple-ring coronas created by mean cloud-particle diameters within a narrow range of approximately 6.5–15 μm. Because their scattering model predicted multiple-ring coronas with mean cloud particles as large as 25 μm, while their photographic analysis inferred drop sizes not exceeding 15 μm, they wondered if perhaps these larger drop sizes were accompanied by a broadening of the drop-size distribution or an increase in multiple scattering, destroying the visibility of multiple-ring coronas. For particles smaller than their 6.5-μm lower limit, their analysis suggested that multiple-ring displays would not be visible because the combination of refracted and diffracted light results in the colors being highly sensitive to particle size, such that any reasonable drop-size distribution destroys the colored rings. Lock and Yang[3] also showed that the simpler Fraun-

J. A. Shaw (jshaw@ece.montana.edu) is with the Department of Electrical and Computer Engineering, Montana State University, Bozeman, Montana 59717. P. J. Neiman is with the National Oceanic and Atmospheric Administration Environmental Technology Laboratory, 325 Broadway, Boulder, Colorado 80305.

Received 29 January 2002; revised manuscript received 29 April 2002.

0003-6935/03/030476-10$15.00/0

Fig. 1. Photograph of iridescent standing lenticular wave clouds above Boulder, Colorado, on 8 November 1995. This cropped photo was taken with a 70–210-mm focal length lens; the exact focal length is unknown.

hofer diffraction theory could be used with results comparable with the Mie scattering calculations, as long as a blue wavelength of 0.49 μm was used for the dominant short wavelength instead of the traditional green 0.57 μm.[1–5] This is in agreement with many of their chromaticity diagrams, which show the principal plane of oscillation being between red and blue coordinates (not red and green).

We find this particularly interesting because, whereas traditionally coronas are described as diffraction phenomena with dominant colors of pink and green, our observations strongly favor pink and blue, at least in mountain wave clouds. We do not believe that previous observations of pink and green coronas and iridescence are in error but rather that there is a fundamental difference in the dominant colors for mountain wave clouds and nonorographic clouds.

Gedzelman and Lock[7] extended the Mie scattering model to include a Rayleigh scattering atmosphere below and above a geometrically thin cloud of variable optical thickness. As with previous simulations,[3] the clouds contain spherical drops of liquid water. This model provides the valuable capability of performing the most-complete simulations yet of coronas and should provide a significant step forward in understanding how variables such as cloud particle size distribution and cloud optical depth combine to create corona displays. The scattering calculations made so far by Gedzelman and Lock[7] suggest that the corona color purity is maximized for a cloud optical depth of 0.2 and becomes effectively zero for a cloud optical depth of 4. They also show that colors other than the first-order ring usually cannot be perceived in very thin clouds (optical depth < 0.05) because of the competing blue daytime skylight. In agreement with this interpretation, we have noted that the most intensely blue multiple-ring coronas occur in extremely thin wave clouds at night, when the visible background is black.[6]

As illustrated in Fig. 1, mountain wave clouds[8–12] can produce particularly vivid coronas and iridescence because of their narrow particle-size distribution and small mean particle sizes.[13–15] Mountain wave clouds, especially of the vertically propagating variety, tend to be geometrically thin in the vertical direction and have a large ratio of horizontal-to-vertical air motion within them. These conditions result in a limited amount of time for cloud particles to fall as they are quickly transported through the wave cloud, which results in such lenticular clouds being optically thin and often lens shaped. In this paper we show photographs of coronas and iridescence observed within mountain wave clouds along the steep lee side of the Rocky Mountains over northeastern Colorado. Such clouds are commonly observed in this location, as well as on the downstream side of many other prominent mountain ranges, and tend to have small cloud particles with narrow particle-size distributions. These conditions lead to relatively frequent, high-quality optical displays (e.g., Fig. 1) that are remarkably more colorful and

intense than what we have seen in nonorographic clouds.

Regardless of the particular cloud type, it has been accepted traditionally that spherical liquid cloud droplets are primarily responsible for coronas and iridescence. For example, in 1912 Simpson[1] reported on corona observations in Antarctica during Captain Scott's first British Antarctic expedition, concluding that supercooled liquid water droplets were the diffracting objects leading to the colorful displays observed in air temperatures ranging from −26 to −29 °C. Simpson's conclusion was based on a combination of corona and fogbow observations that led him to believe that the clouds during that display could not have contained ice crystals. Much later, Sassen[2] analyzed a photograph of iridescence in an airplane contrail, also concluding that the particles involved were most likely liquid water drops and not ice. However, later observations of a corona in a high cirrus cloud exhibiting large depolarization ratios in lidar backscatter led Sassen[4] to conclude that diffraction by unusually small (~25 μm) ice crystals was indeed the source of that corona. Sassen *et al.*[5] described a similar observation and further documented it by collecting and photographing the small ice crystals, collected by an airborne sampler at the top of a high cirrus cloud with a temperature near −70 °C.

In this paper we add further documentation of vivid corona displays being created by small ice-phase cloud particles. In over half our photographs that we describe, the meteorological conditions require the cloud particles to consist of ice, not liquid water, on the basis of the homogeneous freezing point (~−36 °C) of supercooled droplets.[13,14] The unique feature of our observations is that they are all in mountain wave clouds. Microphotographs of particles collected from the interior of similar mountain wave clouds show that such clouds do indeed quite often contain small and monodisperse ice particles, but that these particles are quasispherical with effective diameters less than 25 μm (Fig. 2).[16,17] This small size, much smaller than typical ice crystals in nonorographic clouds, provides a mechanism for the high-quality displays to be generated within wave clouds at high altitudes with temperatures below −36 °C. Therefore our analysis shows that visible diffraction displays caused by such small ice particles are more common than previously documented. Our observations of mean particle sizes from 7.6 to 24.3 μm also help fill in the gap of large-particle multiring coronas in the Lock and Yang[3] observation set. It will be particularly interesting in the future to use scattering models to explore the possible effect of the different complex refractive index of ice and liquid water on the visual appearance of coronas and iridescence.

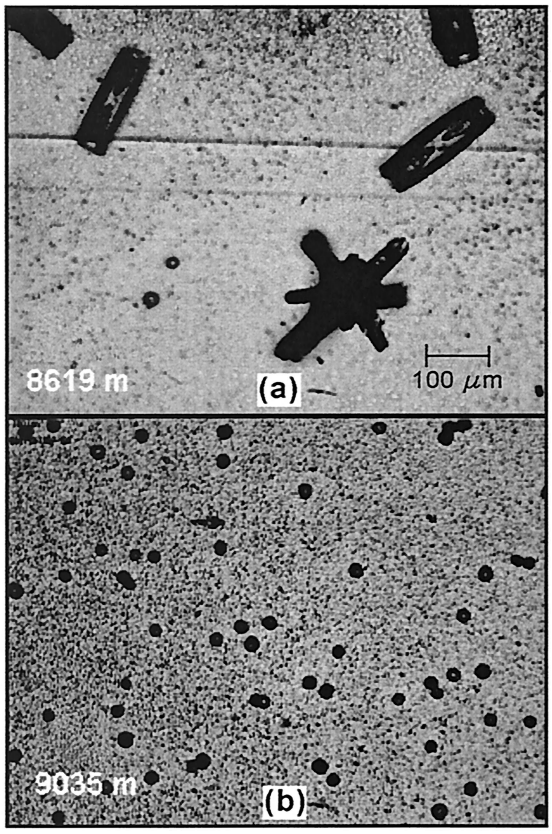

Fig. 2. *In situ* observations of frozen cloud particles in an upper-tropospheric mountain wave cloud at a pressure altitude and temperature of (a) 339.3 mb and −34.4 °C, and (b) 319.3 mb and −40.0°C. The classical ice crystals in (a), whose ~100-μm size is shown for scale, are associated with a nearby nonorographic cirrus cloud, while the much smaller quasispherical particles in (b) are frozen wave-cloud particles (freezing of supercooled droplets on collection can be ruled out because drops larger than a few micrometers cannot exist colder than the homogeneous nucleation point of about −36 °C).[17] These ice particles were collected in mountain wave clouds similar to the ones that produced the optical displays illustrated with photographs in this paper. Photos courtesy of Andy Heymsfield at the National Center for Atmospheric Research, Boulder, Colorado.[17]

2. Diffraction Theory for Corona Analysis

Closed-form solutions of electromagnetic scattering theory generally are limited to special cases, such as particles that have spherical (Mie scatter), cylindrical, or otherwise simple geometry or symmetry.[18] A much simpler approach to modeling coronas, however, is to use scalar diffraction theory, which provides a polarization-independent (scalar) approximate solution for scattering by objects or apertures that are larger than the optical wavelength.[19] Some of the light impinging on such an object is deviated from its prior course, or diffracted, into a new direction that depends on wavelength and object size.

The simplest form of scalar diffraction theory is obtained in the Fraunhofer approximation, valid for diffraction patterns observed at a distance much greater than $\pi d^2/\lambda$, where d is the maximum transverse object dimension (i.e., particle diameter) and λ is the optical wavelength. At such distances, the diffraction pattern is proportional to the spatial Fourier transform of the object. Corona and iridescence

in clouds typically satisfy this condition for ground-based observers.

The irradiance (W m^{-2}) in a Fraunhofer diffraction pattern for a uniformly illuminated circular object of diameter d is described by the Airy function,

$$I(r) = \left(\frac{\pi d^2}{4\lambda z}\right)^2 \left[\frac{2J_1\left(\frac{\pi d r}{\lambda z}\right)}{\left(\frac{\pi d r}{\lambda z}\right)}\right]^2 \quad (1)$$

where r is the radial coordinate in the observation plane (i.e., the radius of the diffraction pattern), λ is the optical wavelength, z is the distance from the diffracting object to the observer, and J_1 is a first-order Bessel function of the first kind. The Airy pattern in Eq. (1) is a set of concentric rings, often described in terms of their angular radius θ (the angle by which the light is deviated upon encountering the particle). Because Fraunhofer theory is valid only for small angles, some sort of small-angle approximation is common, resulting in the Bessel function argument being written in one of the following forms:

$$\frac{\pi d r}{\lambda z} = \frac{\pi d \tan(\theta)}{\lambda} \approx \frac{\pi d \sin(\theta)}{\lambda} \approx \frac{\pi d \theta}{\lambda}. \quad (2)$$

We choose to use the $\sin(\theta)$ version of Eq. (2), describing the angular position of maxima and minima in the oscillating Airy pattern with

$$\sin(\theta) = m\lambda/d, \quad (3)$$

where m is a constant (0, 1.635, 2.679, 3.699, 4.710, . . . for maxima and 1.220, 2.233, 3.238, . . . for minima). Note that, according to Eq. (3), the rings will have shorter-wavelength blue on the inside and longer-wavelength red on the outside. Furthermore, large corona rings result from small particles, whereas small rings result from large particles. Thin clouds minimize multiple scattering and narrow particle-size distributions avoid excessive overlap of colored rings, leading to the best visual displays. Mountain wave clouds often meet these stringent conditions.

In this paper we infer the mean cloud-particle sizes from the measured maxima for red and blue light in corona photographs taken with lenses of known focal length. We use the maxima because we feel it allows us to identify most reliably the wavelength appropriate for any point in the photograph. This approach differs only in minor respects from that of previous studies,[1–5] which describe the approximate angular minima in circular diffraction patterns with $\sin(\theta) = (n + 0.22)\lambda/d$. This equation approximates the angular location of the nth-order minimum, and traditionally has been used with a green wavelength of 0.57 μm, which is assumed to coincide with the red maximum (however, a blue wavelength of 0.49 μm now seems to be more appropriate[3]).

3. Analysis of Corona and Iridescence Photographs

We have observed many displays of corona and iridescence through mountain wave clouds in the vicinity of Boulder and Nederland, Colorado, on the eastern (leeward) edge of the Rocky Mountains, during more than a decade of careful observing. All examples presented in this paper occurred with west-to-northwest flow near mountain top in the layer between 700 and 500 mb (Table 1), or approximately 3.0 to 5.5 km above mean sea level (MSL). The associated cross-mountain (west-to-east) component of this layer-mean flow was significant (7.1 to 17.4 m s^{-1}) and quite likely contributed to the generation of mountain-wave activity and the wave clouds.[8,9,20] We used the heights and temperature ranges of prominent moist layers in soundings at Denver, Colorado, and Grand Junction, Colorado, to deduce the approximate height and temperature characteristics of these wave clouds. It is reasonable to assume, though impossible to confirm, that the wave clouds that produced the diffraction patterns resided within these moist layers, all of which were colder than the melting level (i.e., <0 °C).

These mountain wave clouds are formed by air pushed upward as winds blow across the Continental Divide, usually are optically thin, and tend to have narrower particle-size distributions than other cloud types. Mountain wave clouds typically contain liquid water drops at temperatures down to approximately −36 °C.[14,15] However, when the temperature falls below a threshold near this value, the water particles in these wave clouds freeze rapidly, forming small, quasispherical ice particles with diameters that approach 25 μm. Such ice particles from Colorado mountain wave clouds (Fig. 2)[17] are slightly larger than the original liquid water droplets but are much smaller than typical ice crystals found in nonorographic clouds (sizes $\gtrsim$100 μm).[21–23] These small wave-cloud ice particles have sufficiently spherical shapes to produce coronas that are similar to liquid-generated ones. As far as we know, this is the first documentation of this kind of small quasispherical ice particle coronas in mountain wave clouds.

Figures 3–8 are photographs of six different optical displays in wave clouds on the lee side of the Rocky Mountains near Boulder and Nederland, Colorado. In this subsection we use Eq. (3) from Fraunhofer diffraction theory, along with mean wavelengths of 0.63 and 0.48 μm, to determine the mean particle diameter from the angular radii of the red and the blue coronal rings, respectively [the angular radius for each ring is determined as $\tan^{-1}$(ring radius on the slide/focal length of the lens)]. A common attribute linking these examples, and many other displays that we have observed in mountain wave clouds, is the vividness of the blue color, often at the expense of green. All photographs were taken without neutral-density, polarizer, or other filters other than simple skylight filters used to protect the front lens surface. Unfortunately, we do not have exact exposure data for all photographs, but they all were

Fig. 3. Photograph of a circular corona above Nederland, Colorado, on 5 November 1989. The first-order red ring and the second-order blue and red rings are marked to the right of the Sun, and their radii are labeled in degrees. This cropped photo was taken with a 70-mm focal-length lens.

taken by handheld cameras on 35-mm slide film at reasonably typical exposure time and $F/\#$ settings [for example, the iridescent cloud in Fig. (8b) was photographed at approximately $F/8$ and 1/125 s; corona photographs, especially ones in which the surrounding sky appears very dark, were typically photographed with substantially lower exposure to bring out the colors from the bright light near the Sun].

A. Circular Corona

Figure 3 shows a corona with multiple brightly colored concentric rings, resulting from diffraction in a thin cloud with a highly monodisperse particle-size distribution. The highly uniform colors and circular shape both suggest further that the particle-size distribution was quite uniform throughout this portion of the cloud. The Sun is at the center of the rings, blocked by the top of the tree. To the right of the Sun are numbers that represent the average angular radii (in degrees) of the rings determined for the first-order red ring and the second-order blue and red rings at four locations in the photograph. From Eq. (3) these values correspond to a mean cloud particle size of 20.4 μm ($\pm$0.5 μm), which is comparable to *in situ* aircraft observations of frozen particle sizes within wave clouds.[14,15]

On the basis of the meteorological data summarized in Table 1, this wave cloud could have resided in

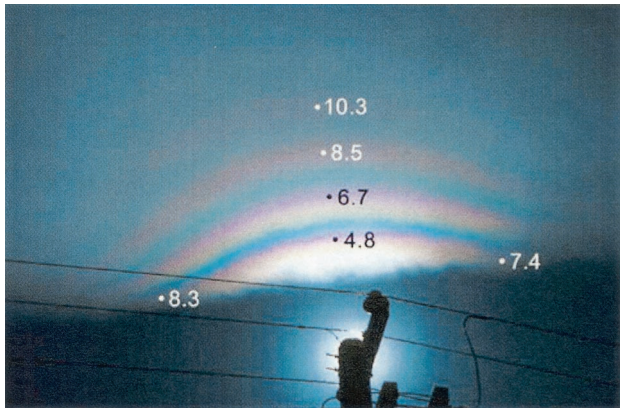

Fig. 5. Photograph of an asymptotic corona at the upwind edge of a wave cloud above Nederland, Colorado, on 31 May 1987. The first-order red ring is marked above and to the sides of the Sun, and the second- through fourth-order red rings are marked above the Sun; their angular radii are labeled in degrees. This cropped photo was taken with a 70-mm focal-length lens.

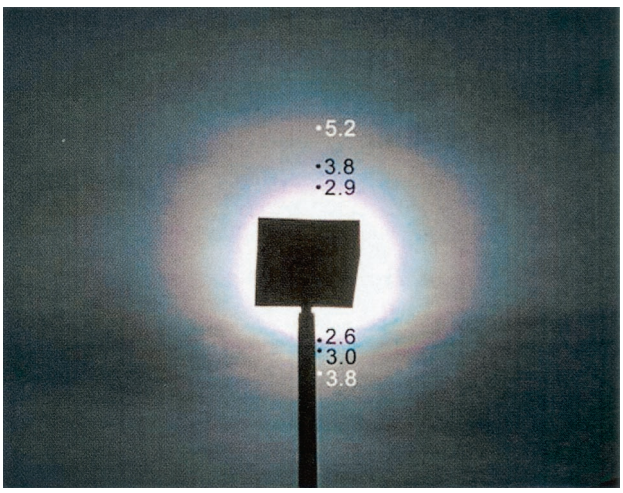

Fig. 4. Photograph of an oblong corona above Boulder, Colorado, on 29 January 1987. The first-order red ring and the second-order blue and red rings are marked below and above the Sun, and their radii are labeled in degrees. This cropped photo was taken with a 70-mm focal-length lens.

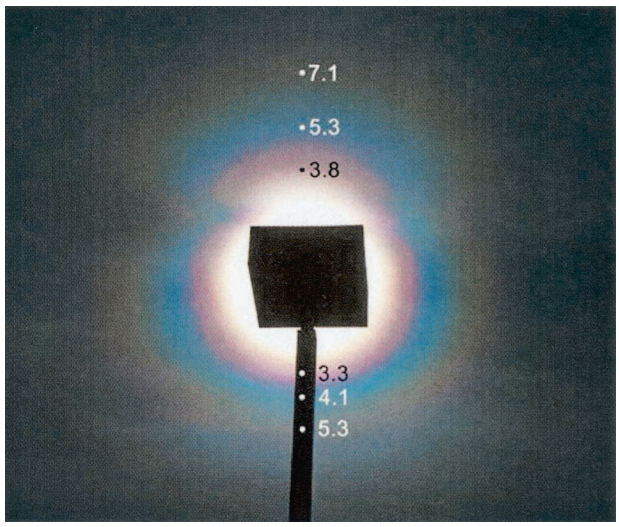

Fig. 6. Photograph of a stepwise discontinuous corona above Boulder, Colorado, on 31 October 1989. The first-order red ring and the second-order blue and red rings are marked below and above the Sun, and their radii are labeled in degrees. This cropped photo was taken with a 70-mm focal-length lens.

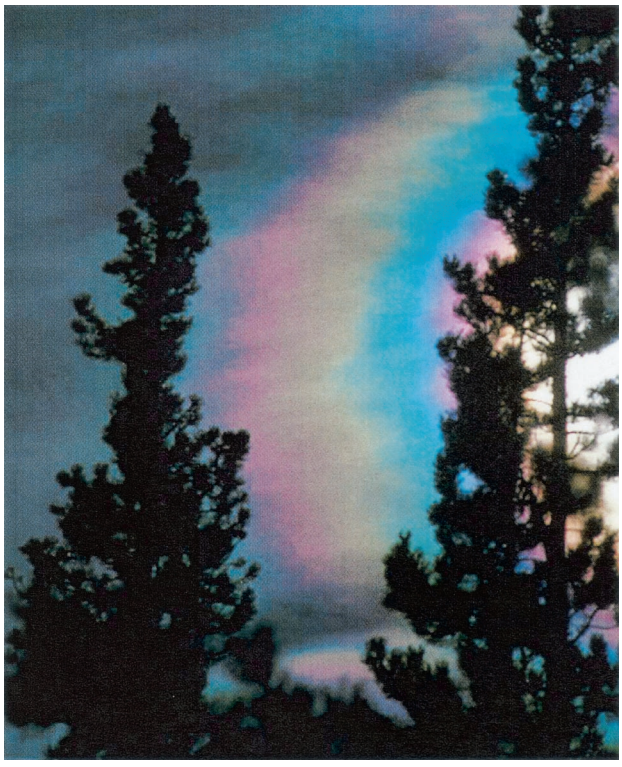

Fig. 7. Photograph of a ragged corona above Nederland, Colorado, on 15 January 1996. This cropped photo was taken with a 70–210-mm focal-length lens; the exact focal length is unknown.

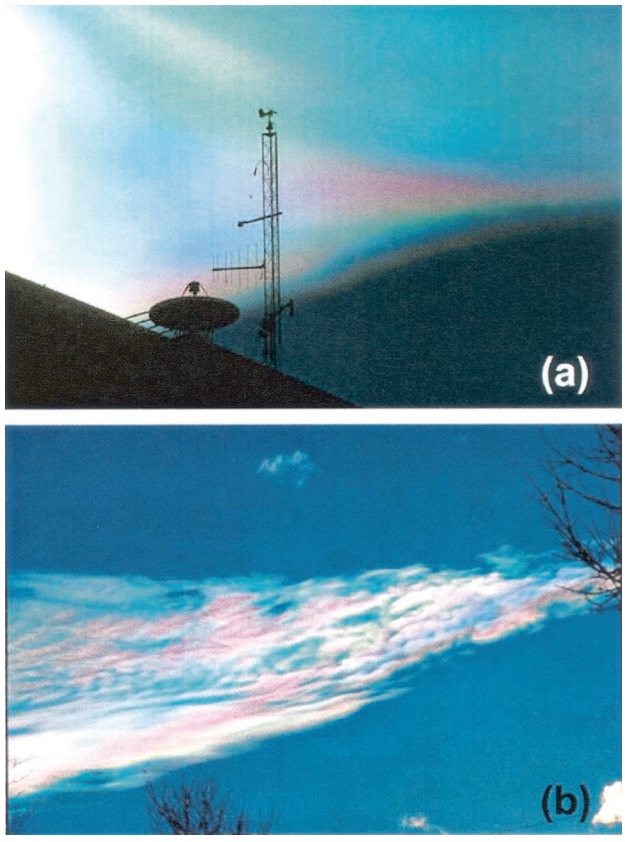

Fig. 8. Photographs of iridescence above Boulder, Colorado, on (a) 8 November 1995 and (b) 25 December 1998. These cropped photos were taken with 70–210- and 28–200-mm focal-length lenses, respectively. The exact focal length in (a) is unknown, and the focal length in (b) is ~120 mm.

one of three layers that extended collectively through a deep layer of the troposphere from ~650 to 320 mb (i.e., from approximately −5 to −40 °C). However, the contrail in this photo can be used to constrain the estimate of the vertical position and temperature of the cloud. Because contrails form at temperatures below approximately −43 °C,[24] we know from the nearby soundings that this contrail could not have resided lower than ~9 km MSL, or ~6.4 km above ground. Furthermore, in the original photograph the contrail cast a sharp but very narrow (<0.3° of arc) shadow on the wave cloud, with the shadow located directly above the contrail and to the left of the Sun, suggesting that the contrail was slightly above the wave cloud in the left portion of the photo and within the cloud on the right side. Knowing that the maximum possible solar angle for the date of the photo is ~33.5° and then performing the appropriate simple geometry, we determined that the contrail could not have extended more than ~25 m above the cloud (this is reasonable since the flow is usually highly laminar and not excessively turbulent in wave clouds away from the wave-breaking region near the tropopause and away from the lower-level rotor circulations). Also, given that the wave cloud was quite thin (i.e., note the sharp detail of the contrail through the wave cloud), the wave cloud effectively resided at the level of the contrail, i.e., at a temperature ≤−43 °C or slightly above the uppermost moist layer measured by the soundings. At these very cold temperatures the wave-cloud particles can exist only in solid form.[13] The relatively large wave-cloud particle size of 20.4 μm inferred from the angular radii of the coronal rings further supports this conclusion. Sassen[4] and Sassen *et al.*[5] previously documented ice-crystal coronas within non-wave-like cirrus cloud sheets, though these displays are relatively uncommon since the ice crystals in cirrus clouds are nonspherical and often too large (i.e., >~100 μm)[21–23] to produce visible coronas.

B. Noncircular Coronas

Wave-cloud particles can be sufficiently uniform in size to produce noticeable diffraction rings, but they may vary enough in size across the cloud that these rings are noncircular. This subsection highlights four variants of noncircular coronas. Where possible, we use Eq. (3) to determine the particle diameter corresponding to the "radius" at different points within the noncircular diffraction pattern.

1. Oblong Corona

The diffraction rings of the oblong-shaped corona in Fig. 4 have a larger diameter at the top of the photograph and become gradually smaller toward the bottom. This is caused by the mean cloud particle sizes becoming steadily larger from top to bottom.

Table 1. Mean Wind, Moisture, and Temperature Characteristics from the Relevant Denver and Grand Junction Rawinsonde Soundings for the Diffraction Displays Shown in Our Photographs[a]

Date (day-month-year)	Fig. No.	700–500-mb Mean Wind Information			Moist Layers[b] (mb)	Temperature Range of Moist Layers (−°C)	Inferred Cloud Particle Size (μm)	Cloud Particle Phase
		Direction (deg)	Speed ($m\ s^{-1}$)	Cross Mountain ($m\ s^{-1}$)				
29-Jan-87	4	301	13.6	11.7	565–429; 400–331	15.5–28.2; 31.9–39.9	19.5–24.3	Ice
31-May-87	5	262	7.2	7.1	638–562; 550–500; 420–363	0.1–8.2; 6.7–9.1; 18.3–25.7	7.6–16.6	Liquid
31-Oct-89	6	283	14.0	13.6	559–493; 474–443; 457–341	6.9–24.5; 23.2–26.1; 24.1–39.8	14.4–18.1	Liquid/ice
05-Nov-89	3	280	17.7	17.4	650–547; 511–386; 450–322	5.1–14.4; 16.0–29.7; 22.0–39.9	20.4	Ice
08-Nov-95	1, 8(a)	294	15.0	13.7	315–100	38.9–70.7	—	Ice
15-Jan-96	7	271	14.4	14.4	552–529; 387–100	12.0–13.6; 31.1–65.2	—	Ice
25-Dec-98	8(b)	310	17.3	13.3	579; 440–420; 300–250	15.9; 30.7–33.5; 52.5–58.3	—	Liquid

[a]Inferred cloud particle sizes are also shown for each display (where applicable), as is the estimated cloud particle phase.
[b]A moist layer is defined by a local minimum in a vertical profile of dewpoint depression.

The mean particle diameters deduced from the angular radii of these rings ranged from 19.5 μm at the top of the corona to 24.3 μm at the bottom. These relatively large sizes suggest that the wave clouds were composed of ice particles, which is supported by the observation that the upper portion of the higher moist layer in nearby soundings was colder than the homogeneous nucleation point. It is unclear precisely why the ice particles gradually changed size across the corona. However, it is possible that this change reflected the growth of ice particles in the upward-motion portion of the wave cloud, especially given that a small component of the upper-tropospheric flow was directed from the top of the corona to the bottom.

Several other authors have documented oblong coronas that appear in a clear sky from diffraction by pollen.[25–27] The shape of these coronas reflects the shape of the pollen spores: circular for juniper, oblong or otherwise asymmetric and noncircular for pine and birch, and so forth. However, the oblong corona described here results from a local gradient in mean cloud particle diameter.

2. *Asymptotic Corona*

The uniquely shaped high-order corona shown in Fig. 5 is an extreme example of a noncircular corona. It contains a series of colored bands at the upwind edge of a wave cloud, whose radii expand continuously (never closing) as the upwind edge is approached from the cloud interior. This sharp spatial gradient in diffraction ring radius indicates rapid particle growth downwind of the cloud edge (i.e., toward the top of the photograph). The angular radii of the first- through fourth-order red rings above the Sun correspond to cloud particle sizes of 12.3, 14.5, 15.8, and 16.6 μm, respectively, while the mean radius of the first-order red ring near the edge of the cloud (to the sides of the Sun) was produced by an average particle size of 7.6 μm. The relatively small size of these particles and the fact that the prominent moist layers remained well below the altitude of the homogeneous nucleation point (Table 1) indicate that the wave cloud was composed of water droplets. Because the upwind edge of the cloud is where the limit of the droplet size goes to zero, the angular radii of the diffraction rings here approach infinity. Therefore, we refer to this particular diffraction display as an asymptotic corona.

The fortuitous location and unique shape of these diffraction rings, in tandem with knowledge from rawinsonde observations that midtropospheric flow of ~10 $m\ s^{-1}$ was directed nearly perpendicular to the cloud edge from bottom to top, provide useful information about the distribution of cloud particles and their mean growth rate at the upwind edge or updraft region of this wave cloud. The decrease in radii of the diffraction rings (i.e., the increase in droplet size) from the upstream edge of the cloud to its interior clearly documented the growth of cloud droplets. Assuming steady horizontal flow of 10 $m\ s^{-1}$ through the wave cloud, the most rapid growth rate occurred at the leading edge of the cloud where droplets initially formed and reached a mean size of 7.6 μm in less than ~5 s. Thereafter the droplets increased in size much more slowly to 16.6 μm in either ~34 or ~70 s, depending on whether the cloud was assumed to reside in the lower or the upper moist layer summarized in Table 1. The initial rapid cloud-droplet growth and subsequent slow growth within the updraft region of the wave cloud's upwind edge is fully consistent with *in situ* aircraft observations of droplet growth in the same region of other liquid-phase wave clouds.[14]

3. *Stepwise Discontinuous Corona*

The corona in Fig. 6 exhibits a step discontinuity in diffraction-ring radius near the top of the corona,

indicating a sudden change of mean cloud-particle size. The relatively circular rings in the lower two-thirds of this corona correspond to a mean particle size of 18.1 μm, a value that is representative of frozen wave-cloud particle sizes. In contrast, the partial rings possessing larger angular radii above the Sun were created by a much smaller mean particle size of 14.4 μm that is more characteristic of wave-cloud water droplets. Multiple moist layers were observed during this event (Table 1), the highest of which extended above the homogeneous nucleation point. Heymsfield and Miloshevich[14] presented *in situ* observations of a rapid change in phase of wave-cloud particles from supercooled liquid to ice, and a corresponding jump in particle size, associated with homogeneous nucleation. Therefore it is plausible that the discrete change in the angular radii of the coronal rings in this photograph marks the location of a phase change from supercooled liquid (larger rings, top) to ice (smaller rings, bottom).

4. *Ragged-Edge Corona*

The use of a zoom lens to photograph the corona in Fig. 7 without recording the exact focal length prevents us from accurately determining the mean cloud-particle sizes that produced this corona. Nevertheless, the photo clearly shows the ragged edges of the diffraction rings. This distinctive trait indicates that the cloud particles were sufficiently uniform in size to produce visible colored rings but that the particles also exhibited enough variability in size across the cloud to create undulations within these rings.

This case is unique among those presented in this section because it was characterized by a superposition of high-level wave clouds east of the Continental Divide and synoptic-scale cirrus (as cold as −51 °C) streaming overhead from southern California (determined from satellite imagery not shown here). The soundings clearly documented this upper-level moisture up to 100 mb or ~−65 °C, as well as a very thin moist layer in the middle troposphere (Table 1). When this photo was taken, however, midtropospheric wave clouds were not evident in the immediate vicinity. Therefore it is quite likely that both the wave clouds and cirrus in the area were composed of ice particles. Because the cirrus was quite cold, its ice crystals might have been small enough to produce a corona[4,5,22] in tandem with the upper-level wave clouds. On the basis of the microphysical characteristics of nonorographic cirrus clouds outlined earlier, we observe the cirrus ice particles in this case to exhibit a comparatively large range of sizes relative to wave-cloud ice particles, and they probably were nonspherical and randomly oriented. Therefore the cirrus ice crystals were quite likely responsible for the ragged appearance of the coronal rings.

C. Iridescence

When sunlight or moonlight passes through a translucent cloud containing clusters of uniformly sized small particles, and each cluster is characterized by a unique mean particle size, a patchwork of colors known as iridescence can be produced, sometimes relatively far from the light source. Iridescence may also occur by means of anomalous diffraction arising from interference effects associated with sunlight or moonlight passing through a cloud composed of very small particle sizes, thus resulting in irregular color patterns quite far from the light source.[3] The two iridescence displays shown in Fig. 8 were distinguished by smooth and mottled cloud textures, respectively. During the first display [Fig. 8(a)], a photo was also taken of iridescent wave clouds in their entirety (Fig. 1). During this display moist conditions existed only at high levels where the temperature was colder than the homogeneous nucleation point (Table 1). These rawinsonde observations are supported by infrared satellite imagery (not shown), showing a localized north–south-oriented wave-cloud band east of the Continental Divide over Boulder with cloud-top temperatures of −52 to −58°C. Hence the iridescence in Figs. 8(a) and 1 were almost certainly produced by ice particles. As is often the case with iridescence, green is more apparent than in many mountain wave-cloud coronas, but all three iridescence photographs in Figs. 1 and 8 also exhibit a significant amount of blue.

Rawinsonde measurements relevant to the display shown in Fig. 8(b) reveal two moist layers that were warmer than the homogeneous nucleation point and one layer that was colder (Table 1). Our qualitative impression was that during this display the iridescent cloud was situated no higher than the middle troposphere, i.e., in a layer where supercooled droplets would have existed. In all three iridescence photos [Figs. 1, 8(a), 8(b)], iridescent colors were observed at least 10°–15° from the Sun, indicating that the cloud particles producing these displays were quite small (i.e., the result of large-angle and possibly high-order diffraction). The corona rings showcased earlier in this paper subtended smaller angles relative to the Sun, indicating larger particle sizes.

4. Discussion and Conclusions

The meteorological conditions for the wave-cloud diffraction displays shown here strongly suggest that in most cases the diffracting objects were small quasispherical ice particles with mean sizes of approximately 7–25 μm (only several of these examples are likely generated by supercooled liquid water). Previous documentation of coronas produced by ice particles are limited to observations in cirrus clouds that appear to be composed of small ice crystals,[4,5] whereas our observations suggest that corona and iridescence quite often can be created by tiny quasispherical ice particles that might be unique to mountain wave clouds (we discuss mountain wave-cloud microphysics in more detail in a similar manuscript being prepared as a review of coronas and iridescence for the meteorological community[28]). Furthermore, the quasispherical shape of these tiny ice particles may not produce a significant depolarization signature, meaning that remote identification of these

wave-cloud ice particles may require techniques other than polarization lidar alone.

The particle diameters that we infer from corona photographs agree well within the particle-size boundaries suggested by Lock and Yang[3] at the small end, but we have several cases of inferred particle diameters significantly larger than the 15-μm upper limit of their observations. This, in fact, helps fill in the large-particle region where the modeling of Lock and Yang[3] predicted that good visible coronas could be created, but for which they found no photographic evidence.

Even beyond the examples included in this paper, our observations (mostly in mountain wave clouds) favor blue over green as the dominant shortwave corona color, but many comments in the community and the popular literature favor green. The blue preference may be unique to diffraction in mountain wave clouds. We see a tendency for iridescence displays to have more green content than coronas, even in mountain wave clouds; sometimes the green is accompanied by blue, but sometimes—especially when the clouds appear to be composed of liquid water—there is significantly less blue. In wave clouds that appear to be extremely thin and high in the atmosphere, the resulting coronas almost always appear as vivid blue rings, rarely exhibiting any green at all. The most striking examples of these blue coronas occur in thin wave clouds at night, with the full or nearly full moon as the light source.

We believe that further observation and modeling will provide much more insight into the cloud microphysics accompanying corona and iridescence displays and into the perceived optical nature of these displays. In particular, we wonder whether there is a connection between the cloud particle-size distribution, or perhaps the type of cloud particle involved, and the perceived short-wavelength dominant color (green versus blue). Given that previous scattering models of coronas have been for liquid spheres, whereas many of the larger particles in our examples appear to be quasispherical ice particles, there is clearly an opportunity to explore what effect the differing refractive indices of ice and liquid water might have on the color and visibility of coronas. However, any such effect will likely be limited to the smallest particles, for which reflection, transmission, and diffraction by the particles tend to be comparable. This analysis will require a scattering formulation instead of diffraction analysis, because diffraction theory considers only the shape and size of the objects and not their optical properties. This future research should be accompanied by a quantitative analysis of the colorimetric properties of coronas and iridescence in mountain wave clouds and other cloud types.

The authors thank Andy Heymsfield (National Center for Atmospheric Research) for providing the wave-cloud particle microphotograph in Fig. 2 and for insightful discussions about wave-cloud microphysics, Ken Sassen (University of Alaska) and Stan Gedzelman (City University of New York) for engaging us in stimulating discussions of coronas and iridescence, and Jim Churnside [National Oceanic and Atmospheric Administration (NOAA)/Environmental Technology Laboratory] and two reviewers for providing helpful and encouraging suggestions for the manuscript. J. A. Shaw acknowledges support from a NOAA Presidential Early Career Award for Scientists and Engineers for his participation in this study.

References

1. G. C. Simpson, "Coronae and iridescent clouds," Q. J. R. Meteorol. Soc. **38,** 291–299 (1912).
2. K. Sassen, "Iridescence in an aircraft contrail," J. Opt. Soc. Am. **69,** 1080–1084 (1979).
3. J. A. Lock and L. Yang, "Mie theory of the corona," Appl. Opt. **30,** 3408–3414 (1991).
4. K. Sassen, "Corona-producing cirrus cloud properties derived from polarization lidar and photographic analyses," Appl. Opt. **30,** 3421–3428 (1991).
5. K. Sassen, G. G. Mace, J. Hallett, and M. R. Poellot, "Corona-producing ice clouds: a case study of a cold mid-latitude cirrus layer," Appl. Opt. **37,** 1477–1485 (1998).
6. J. A. Shaw, "The Christmas corona," Opt. Photon. News (April 1997), pp. 52–53.
7. S. D. Gedzelman and J. A. Lock, "Simulating coronas in color," Appl. Opt. **42,** 497–504 (2003).
8. R. B. Smith, "The influence of the mountains on the atmosphere," in *Advances in Geophysics,* B. Saltzman, ed. (Academic, New York, 1979), vol. 21, pp. 87–230.
9. D. R. Durran, *Mesoscale Meteorology and Forecasting,* P.S. Ray, ed. (American Meteorological Society, Boston, 1986), pp. 472–492.
10. T. Q. Carney, A. J. Bedard, Jr., J. M. Brown, J. McGinley, T. Lindholm, and M. J. Kraus, *Hazardous Mountain Winds and Their Visual Indicators,* NOAA Handbook (Environmental Research Laboratories, Boulder, Colo., 1996).
11. F. M. Ralph, P. J. Neiman, T. L. Keller, D. Levinson, and L. S. Fedor, "Observations, simulations, and analysis of nonstationary trapped lee waves," J. Atmos. Sci. **54,** 1308–1333 (1997).
12. C. D. Whiteman, *Mountain Meteorology: Fundamentals and Applications* (Oxford U. Press, New York, 2000).
13. H. R. Pruppacher and J. D. Klett, *Microphysics of Clouds and Precipitation* (Reidel, Boston, 1980).
14. A. J. Heymsfield and L. M. Miloshevich, "Homogeneous nucleation and supercooled liquid water in orographic wave clouds," J. Atmos. Sci. **50,** 2335–2353 (1993).
15. A. J. Heymsfield and L. M. Miloshevich, "Relative humidity and temperature influences on cirrus formation and evolution: observations from wave clouds and FIRE II," J. Atmos. Sci. **52,** 4302–4326 (1995).
16. H. Gerber, C. H. Twohy, B. Gandrud, A. J. Heymsfield, G. M. McFarquhar, P. J. DeMott, and D. C. Rogers, "Measurements of wave-cloud microphysical properties with two new aircraft probes," Geophys. Res. Lett. **25,** 1117–1120 (1998).
17. A. Heymsfield, Mesoscale and Microscale Meteorology Division, National Center for Atmospheric Research, 3450 Mitchell Lane, Boulder, Colo. 80301 (personal communication, 2001).
18. C. F. Bohren and D. R. Huffman, *Absorption and Scattering of Light by Small Particles* (Wiley, New York, 1983).
19. J. W. Goodman, *Introduction to Fourier Optics*, 2nd ed. (McGraw-Hill, New York, 1996).
20. P. Queney, "The problem of airflow over mountains: a summary of theoretical studies," Bull. Am. Meteorol. Soc. **29,** 16–26 (1948).

21. A. J. Heymsfield and C. M. R. Platt, "Parameterization of the particle size spectrum of ice clouds in terms of the ambient temperature and ice water content," J. Atmos. Sci. **41,** 846–855 (1984).
22. C. M. R. Platt, J. D. Spinhirne, and W. D. Hart, "Optical and microphysical properties of a cold cirrus cloud: evidence for regions of small ice particles," J. Geophys. Res. **94,** 11151–11164 (1989).
23. K. Sassen, D. O. Starr, and T. Uttal, "Mesoscale and microscale structure of cirrus clouds: three case studies," J. Atmos. Sci. **46,** 371–386 (1989).
24. J. Appleman, "The formation of exhaust condensation trails by jet aircraft," Bull. Am. Meteorol. Soc. **34,** 14–20 (1953).
25. P. Parviainen, C. F. Bohren, and V. Makela, "Vertical elliptial coronas caused by pollen," Appl. Opt. **33,** 4548–4554 (1994).
26. E. Trankle and B. Mielke, "Simulation and analysis of pollen coronas," Appl. Opt. **33,** 4552–4562 (1994).
27. F. M. Mims, "Solar corona caused by juniper pollen in Texas," Appl. Opt. **37,** 1486–1488 (1998).
28. P. J. Neiman and J. A. Shaw are preparing a manuscript to be called "Optical diffraction patterns in mountain wave clouds over northeastern Colorado."